Supporting Information

Transition Metal Embedded Boron Doped Graphene for Reduction of CO_2 to HCOOH

Sudatta Giri, Purushothaman M, Debolina Misra*

Materials Modeling and Simulation Laboratory, Department of Physics, Indian Institute of Information Technology, Design and Manufacturing, Kancheepuram, Chennai, India, 600127

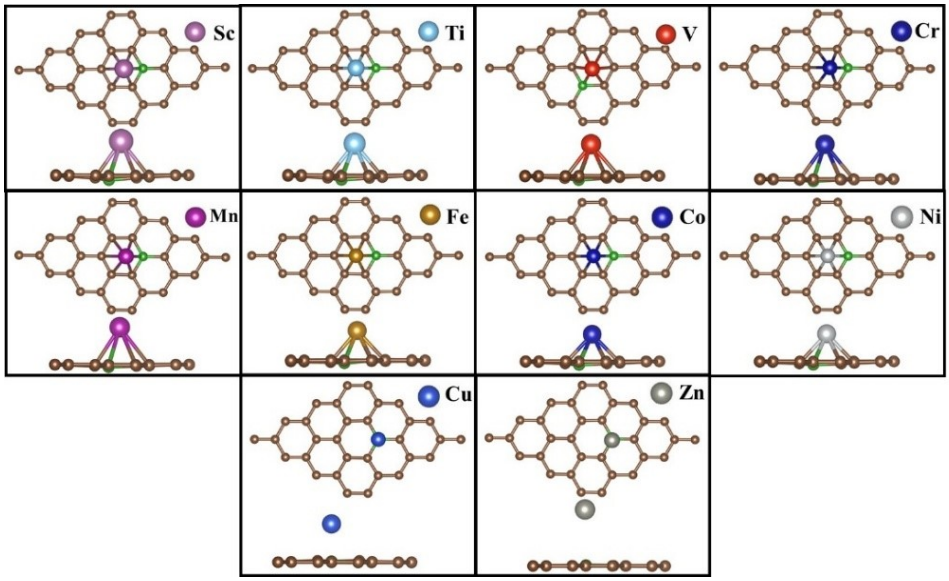

Figure S1: Optimized structures of the TM SAs in their respective preferred doping sites.

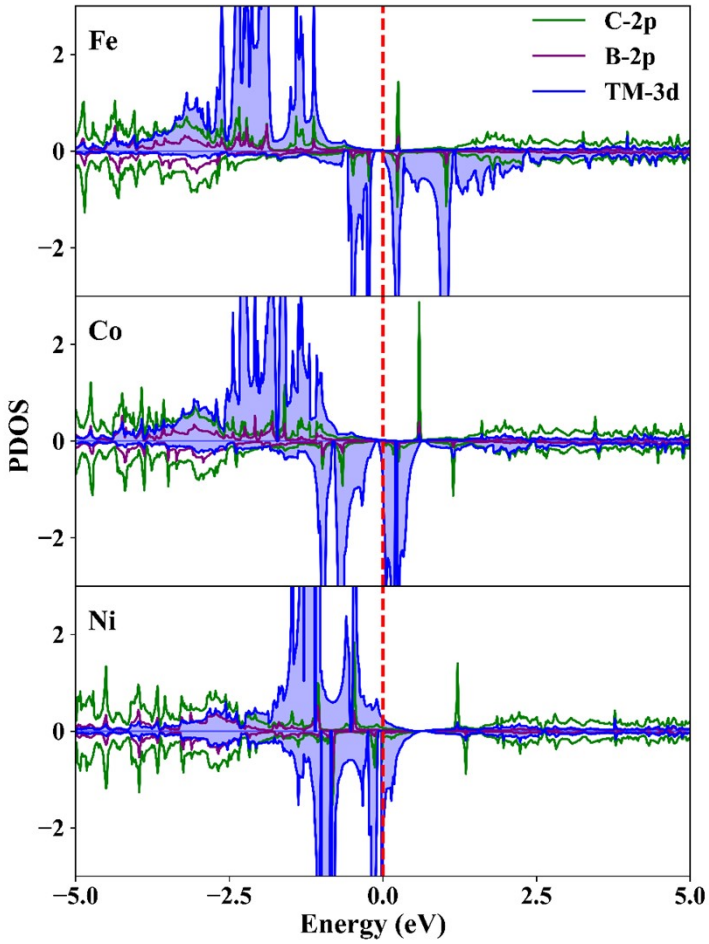

Figure S2: Projected density of states (PDOS) of the TM@B-Gr catalysts (TM = Fe, Co and Ni). Red dotted line is the fermi level.

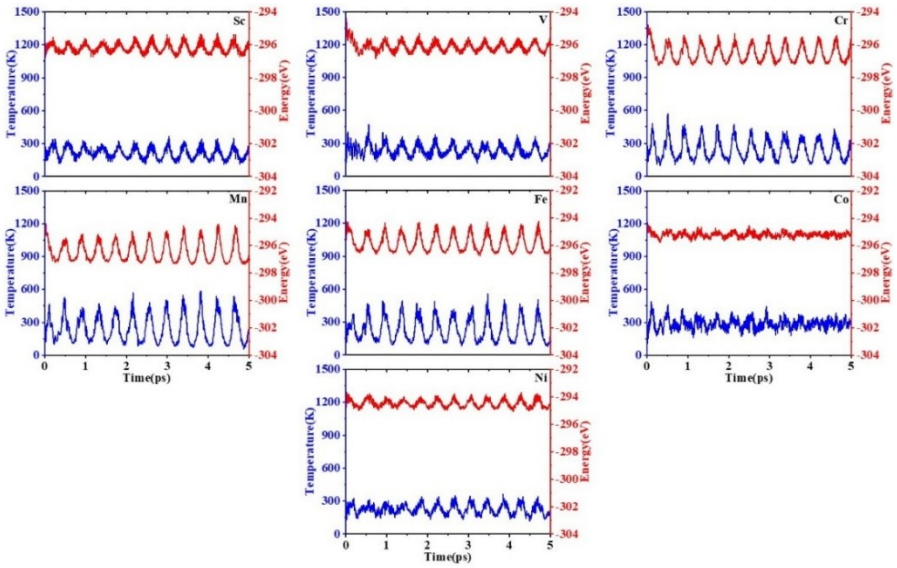

Figure S3: Energy variations with time in Ab Initio Molecular Dynamics (AIMD) simulation for 5 ps at 300 K on TM@B-Gr.

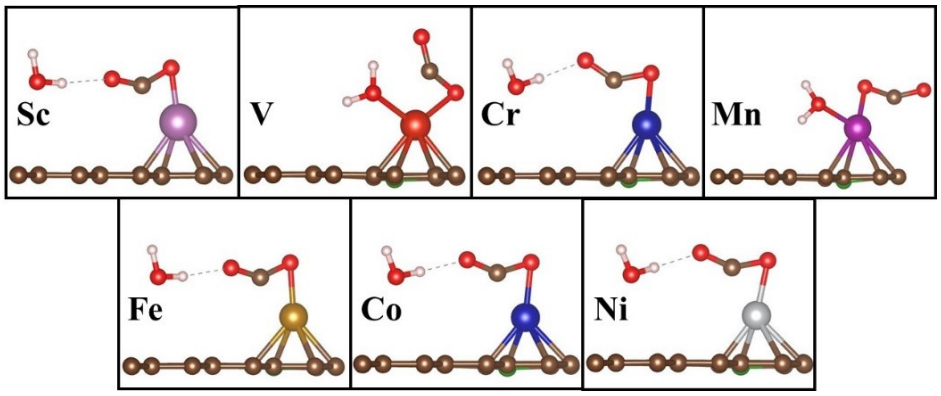

Figure S4: CO_2 and H_2O co-adsorption on TM@B-Gr.

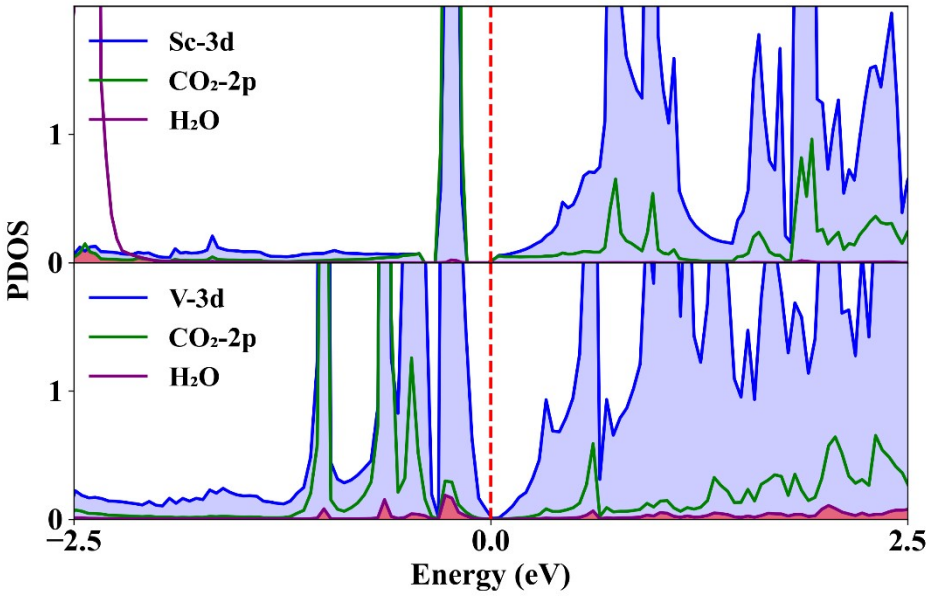

Figure S5: Projected density of states (PDOS) of TM-3d, CO_2-2p and H_2O for Sc- and V@B-Gr.

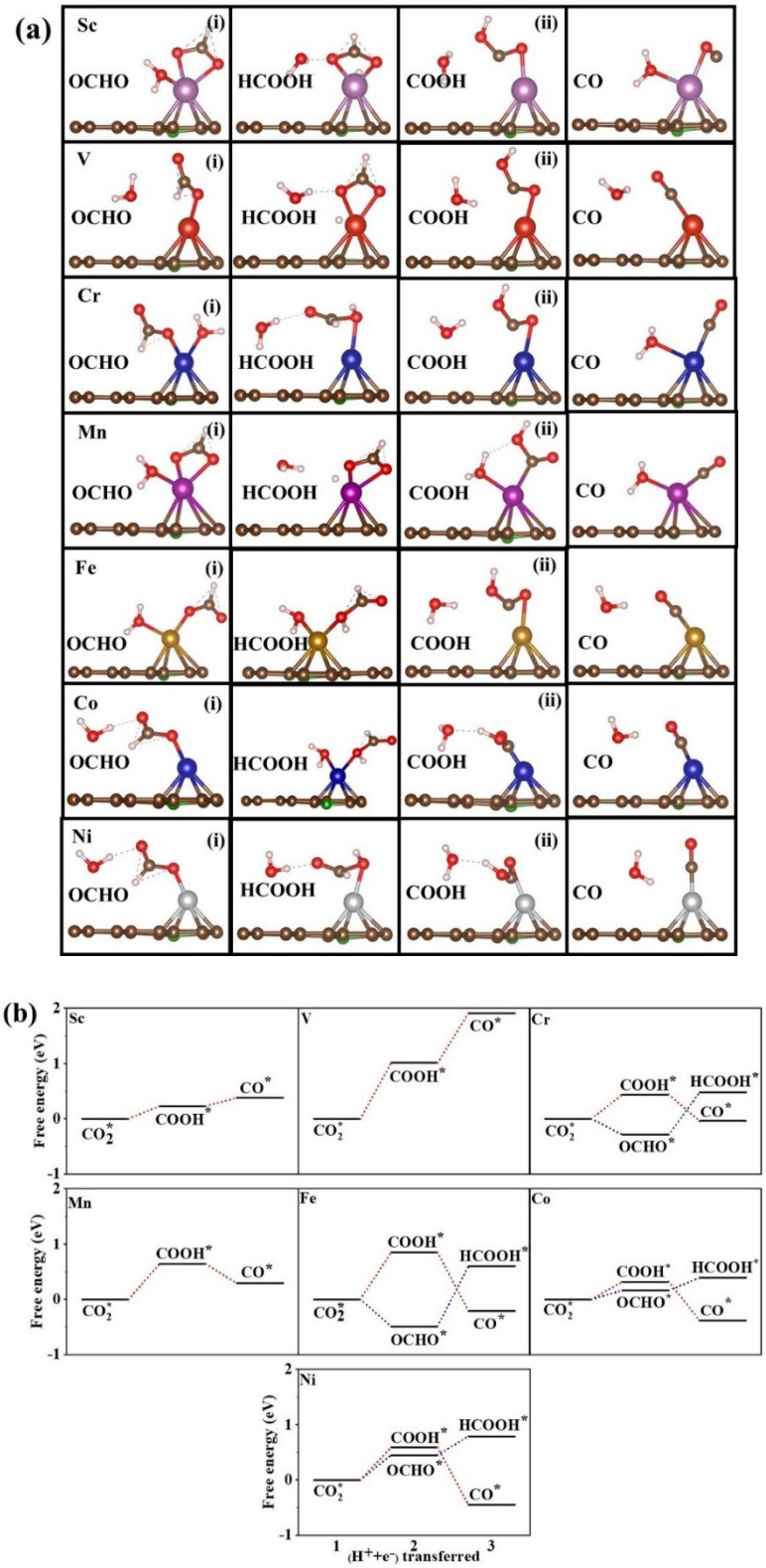

Figure S6: (a) DFT-optimized structural geometries for preferred reaction pathway and **(b)** Free energy profiles for two PCET CO_2RR pathway in presence of H_2O on TM@B-Gr.

TM	BE (eV)
Sc	-3.81
Ti	-4.02
V	-3.42
Cr	-2.37
Mn	-2.04
Fe	-2.97
Co	-3.86
Ni	-3.51
Cu	-2.51
Zn	-0.15

Table S1: Binding energy of TM SAs in presence of H_2O.

Adsorbate	ZPE (eV)	-TS (eV)	G – E_{elec} (eV)
CO_2^*	0.330	-0.255	0.075
$COOH^*$	0.619	-0.098	0.521
CO^*	0.219	-0.131	0.088
$OCHO^*$	0.592	-0.158	0.434
$HCOOH^*$	0.940	-0.150	0.790

Table S2: Contributions of zero-point energy and entropic corrections to adsorbate free energies[1,2].

TM	H-Adsorption	
	E_{ads} (eV)	ΔG (eV)
Sc	2.283	2.523
V	2.057	2.297
Cr	-0.336	-0.096
Mn	-0.761	-0.521
Fe	-0.698	-0.458
Co	-0.229	0.011
Ni	-0.198	0.042

Table S3: Adsorption energies and free energies for H-adsorption on TM@B-Gr catalysts.

TM	DFT						DFT+U		
	d_{TM-O} (Å)	<O-C-O	O—C (Å)	E_{ads}^{CO2} (eV)	ΔG^{CO2} (eV)	q_{CO2} (*e*)	E_{ads}^{CO2} (eV)	ΔG^{CO2} (eV)	q_{CO2} (*e*)
Sc	1.90	141	1.29	-0.87	-0.19	-0.99	-0.62	-0.06	-0.84
V	2.03	140	1.29	-1.45	-0.77	-0.81			
Cr	1.88	133	1.33	-0.39	0.29	-0.81			
Mn	1.98	141	1.29	-1.26	-0.58	-0.64			
Fe	1.90	141	1.29	-0.55	0.13	-0.57	-0.24	0.44	-0.51
Co	1.90	142	1.28	-0.32	0.36	-0.54			
Ni	1.92	145	1.27	-0.47	0.21	-0.46			

Table S4: TM—O (O of CO_2 molecule) and O—C bond length, O-C-O bond angles, bader charge for CO_2, adsorption energy (E_{ads}), adsorption free energies (ΔG) of CO_2 in presence of H_2O.

TM	DFT				DFT+U			
	COOH		OCHO		COOH		OCHO	
	E_{ads} (eV)	ΔG (eV)	E_{ads} (eV)	ΔG (eV)	E_{ads} (eV)	ΔG (eV)	E_{ads} (eV)	ΔG (eV)
Sc	-3.13	0.23	-5.75	-2.26	-3.03	0.07	-5.72	-2.47
V	-2.93	1.01	-3.65	0.42				
Cr	-2.44	0.44	-3.94	-0.93				
Mn	-3.01	0.64	-4.68	-0.80				
Fe	-2.19	0.85	-3.67	-0.49	-1.73	1.00	-3.95	-1.00
Co	-2.48	0.32	-2.79	0.16				
Ni	-2.37	0.59	-2.65	0.45				

TM	DFT				DFT+U			
	CO		HCOOH		CO		HCOOH	
	E_{ads} (eV)	ΔG (eV)	E_{ads} (eV)	ΔG (eV)	E_{ads} (eV)	ΔG (eV)	E_{ads} (eV)	ΔG (eV)
Sc	-1.36	0.15	-	-	-1.28	0.14	-	-
V	-1.01	0.90	-	-				
Cr	-1.30	-0.48	-0.19	1.81				
Mn	-1.84	-0.35	-	-				
Fe	-1.63	-1.06	-0.63	1.09	-1.23	-1.12	-0.65	1.35
Co	-1.56	-0.70	-0.62	0.23				
Ni	-1.80	-1.04	-0.36	0.34				

Table S5: Adsorption energies and free energies for different intermediates on TM@B-Gr in presence of H_2O.

System	U_L (V)	PDS
V@B-Gr[This work]	-0.22	$COOH^* \rightarrow CO^*$
Co@B-Gr[This work]	-0.60	$OCHO^* \rightarrow HCOOH^*$
Ni@B-Gr[This work]	-0.57	$CO_2^* \rightarrow COOH^*$
Co-N_4@Gr[2]	-0.69	$CO_2 \rightarrow COOH^*$
Ni-N_4@Gr[2]	-1.51	$CO_2 \rightarrow OCHO^*$
NiN4@Gr[3]	-1.01	$CO_2 \rightarrow COOH^*$
VN_4[4]	-1.03	$OCHO^* \rightarrow HCOOH^*$
VN_4-GN[4]	-1.19	$OCHO^* \rightarrow HCOOH^*$
Ni-N_2@Gr[5]	-0.63	$CO_2 \rightarrow COOH^*$
Ni-N_3@Gr[5]	-0.62	$CO_2 \rightarrow COOH^*$
Ni-N_4@Gr[5]	-1.29	$CO_2 \rightarrow COOH^*$
Co-GN_4[6]	-0.72	$CO_2 \rightarrow COOH^*$
V-N_4[7]	-0.84	$COOH^* \rightarrow CO^*$
Ni-N_4[7]	-1.35	$CO_2 \rightarrow OCHO^*$
Ni-N_1C_2[8]	-0.94	$CO_2 \rightarrow COOH^*$
Ni-N_3C_1[8]	-0.83	$CO_2 \rightarrow COOH^*$

Table S6: Comparison of limiting potentials (U_L) for CO_2 reduction on TM@B-Gr and TM@N-Gr catalysts.

References:

[1] S. Zhou, W. Pei, J. Zhao, A. Du, Silicene catalysts for CO_2 hydrogenation: the number of layers controls selectivity, Nanoscale 11 (2019) 7734–7743. https://doi.org/10.1039/C9NR01336A.

[2] Y. Yang, J. Li, C. Zhang, Z. Yang, P. Sun, S. Liu, Q. Cao, Theoretical Insights into Nitrogen-Doped Graphene-Supported Fe, Co, and Ni as Single-Atom Catalysts for CO_2 Reduction Reaction, J. Phys. Chem. C 126 (2022) 4338–4346. https://doi.org/10.1021/acs.jpcc.1c09740.

[3] A. Tripathi, R. Thapa, Optimizing CO_2RR selectivity on single atom catalysts using graphical construction and identification of energy descriptor, Carbon 208 (2023) 330–337. https://doi.org/10.1016/j.carbon.2023.03.065.

[4] Z. Yang, Z. Cao, L. Cheng, K. Li, Y. Wang, Z. Wu, Theoretical study on the influence of the extra N in transition metal-N4 embedded graphene as efficient CO_2 reduction catalysts, Applied Surface Science 616 (2023) 156494. https://doi.org/10.1016/j.apsusc.2023.156494.

[5] C. Guo, T. Zhang, X. Liang, X. Deng, W. Guo, Z. Wang, X. Lu, C.-M.L. Wu, Single transition metal atoms on nitrogen-doped carbon for CO_2 electrocatalytic reduction: CO production or further CO reduction?, Applied Surface Science 533 (2020) 147466. https://doi.org/10.1016/j.apsusc.2020.147466.

[6] Z. Lou, W. Li, H. Yuan, Y. Hou, H. Yang, H. Wang, Structural rule of N-coordinated single-atom catalysts for electrochemical CO_2 reduction, J. Mater. Chem. A 10 (2022) 3585–3594. https://doi.org/10.1039/D1TA09015A.

[7] X. Wang, H. Niu, X. Wan, J. Wang, C. Kuai, Z. Zhang, Y. Guo, Identifying TM-N4 active sites for selective CO_2-to-CH_4 conversion: A computational study, Applied Surface Science 582 (2022) 152470. https://doi.org/10.1016/j.apsusc.2022.152470.

[8] Y. Meng, L. Ying, Y. Tao, L. Ma, B. Li, Y. Xing, X. Liu, Y. Ma, X. Wen, DFT Study on Effect of Metal Type and Coordination Environment on CO_2 ECR to C_1 Products over M–N–C Catalysts, Langmuir 40 (2024) 10663–10675. https://doi.org/10.1021/acs.langmuir.4c00590.